A single Einstein–Dilaton geometry linking hadron spectra, galaxy rotation curves, and cosmological growth

Adrian Bohoyo
Systems Architect (R&D), Monfragüe, Spain
ORCID: 0009-0003-1833-4519
Email: rydbergphotonic1@proton.me

29 December 2025

ABSTRACT
A single five-dimensional Einstein–Dilaton background is considered through a frozen solution that provides the warp factor and scalar profile on a finite radial domain. Three independent observables are extracted from the same background without sector-specific retuning: (i) the scalar 0^{++} glueball ratio from the gauge-invariant fluctuation operator ζ, (ii) galactic rotation curves on the SPARC compilation using a single geometry and a single set of global readout parameters (no per-galaxy tuning), and (iii) the linear growth observable $f\sigma_8(z)$ inferred from the same geometry and compared to a flat ΛCDM reference. The gauge-invariant ratio is found to be $m_1/m_0 = 1.5455$ and remains invariant under a coordinate change between the domain-wall coordinate u and conformal coordinate z; the value lies within the standard lattice-QCD band with sub-percent accuracy. An absolute Yang–Mills scale is obtained from the same geometry by evaluating an effective string tension from the infrared warp factor using the standard holographic Wilson-loop relation, yielding a scalar glueball mass $m_0 \simeq 1.6$ GeV for a universal α' choice. On SPARC (175 galaxies), the median χ^2 is reduced relative to Newtonian gravity in the same evaluation protocol, while using only baryonic inputs and the frozen background. For cosmological growth, the BOSS DR12 covariance comparison yields $\chi^2_{\rm ED} \approx 2.27$ and $\chi^2_{\Lambda\rm CDM} \approx 2.44$ (statistically indistinguishable at $z \leq 0.6$), while a high-redshift suppression of order 10% is predicted at $z \simeq 1$ as a falsifiable signature.

Key words: Einstein–Dilaton – holography – galaxies: kinematics and dynamics – cosmology: large-scale structure of Universe – methods: numerical

1 INTRODUCTION

A confining Yang–Mills background is characterized by both dimensionless spectral ratios and an absolute mass scale. For phenomenology across scales, the same background must also provide a consistent galaxy-scale response and an expansion/growth history compatible with large-scale structure data. A single frozen Einstein–Dilaton geometry is analyzed, and three observables are derived: a gauge-invariant scalar glueball spectrum, galaxy rotation curves on SPARC, and the linear growth observable $f\sigma_8(z)$.

2 EINSTEIN–DILATON BACKGROUND AND TRACE

An Einstein–Dilaton (ED) background may be written as

$$S = \frac{1}{2\kappa^2}\int d^5x\,\sqrt{-g}\left[R - \frac{1}{2}(\partial\phi)^2 - V(\phi)\right], \tag{1}$$

evaluated on a domain-wall ansatz,

$$ds^2 = e^{2A(z)}\left(-dt^2 + d\vec{x}^{\,2}\right) + dz^2, \qquad \phi = \phi(z), \tag{2}$$

where $A(z)$ and $\phi(z)$ define the frozen background geometry. The same background functions enter all three sectors below.

3 NUMERICAL TRACE (FROZEN BACKGROUND)

The Einstein–Dilaton equations defining the background constitute a stiff boundary-value problem on a finite radial domain. The frozen trace used here provides sampled arrays

$$\{z,\, A(z),\, A'(z),\, \phi(z),\, \phi'(z)\}$$

together with a diagnostic constraint residual. The domain and resolution are fixed once for all readouts: $z_{\min} = 0.01$ to $z_{\max} = 2.0$ with 1999 grid points. The maximum reported constraint residual is 1.81 on that domain. No sector-specific retuning is performed after this trace is fixed.

4 ANALYTIC RECONSTRUCTION OF THE ED BULK

An analytic reconstruction of the frozen background can be obtained by enforcing the Hamiltonian constraint as a holonomic condition. For the polynomial potential used in the frozen numerical ED background,

$$V(\phi) = -\frac{12}{L^2} - \frac{m^2}{2}\phi^2, \qquad (L = 1,\ m^2 = -3), \tag{3}$$

the constraint

$$H(z) = 12A'(z)^2 - \frac{1}{2}\phi'(z)^2 + V(\phi(z)) = 0 \tag{4}$$

fixes $A'(z)$ once $\phi(z)$ is specified.

A minimal special-function ansatz capturing the observed sign change in the scalar profile is

$$\phi(z) = p_0 + p_1 z + c_0 K_0(k_0 z) + c_1 K_1(k_1 z), \tag{5}$$

with modified Bessel functions K_ν. The warp-factor derivative is then reconstructed on the UV-to-IR branch as

$$A'(z) = -\sqrt{\frac{\frac{1}{2}\phi'(z)^2 - V(\phi(z))}{12}}, \tag{6}$$

and $A(z)$ follows by quadrature up to an additive constant. Using the frozen trace to determine the coefficients yields a primary holonomic fit with

$$p_0 = 1.84795 \times 10^{-2},$$
$$p_1 = -3.04897 \times 10^{-2},$$
$$c_0 = -4.25777 \times 10^{-3},$$
$$k_0 = 6.02488 \times 10^{-1},$$
$$c_1 = 1.16093 \times 10^{-5},$$
$$k_1 = 2.32895 \times 10^{-1},$$

and an analytic zero-crossing $z_\star$ defined by $\phi(z_\star) = 0$ at

$$z_\star \simeq 0.385. \tag{7}$$

By construction, Eq. (6) enforces $H(z) = 0$ for the reconstructed pair $\{A(z), \phi(z)\}$, providing a closed-form representation consistent with the frozen numerical background.

5 DATA AND EVALUATION PROTOCOL

SPARC rotation curves. SPARC provides, for each galaxy, a radial grid r and a baryonic decomposition giving $v_{\rm bar}(r)$ from gas, disk, and bulge components (Lelli et al. 2016). Observed velocities $v_{\rm obs}(r)$ and their reported uncertainties are used only for goodness-of-fit evaluation and visualization. The SPARC comparison uses a single, globally fixed parameter set shared by the full sample; no per-galaxy parameter freedom is introduced. A velocity-weighted goodness-of-fit statistic is reported:

$$\chi^2_{\rm rank} = \sum_i \frac{[v_{\rm model}(r_i) - v_{\rm obs}(r_i)]^2}{v_{\rm obs}(r_i)^2 + 1}, \tag{8}$$

used only as a uniform ranking metric across models under the same protocol. The additive term corresponds to a $(1\,{\rm km\,s^{-1}})^2$ regularization that prevents overweighting very low-velocity points. In addition, a conventional uncertainty-weighted statistic is reported using the SPARC-provided velocity uncertainty σ_i,

$$\chi^2_\sigma = \sum_i \frac{[v_{\rm model}(r_i) - v_{\rm obs}(r_i)]^2}{\sigma_i^2}, \tag{9}$$

reported as a non-reduced statistic to check that qualitative comparisons are not an artefact of the ranking choice.

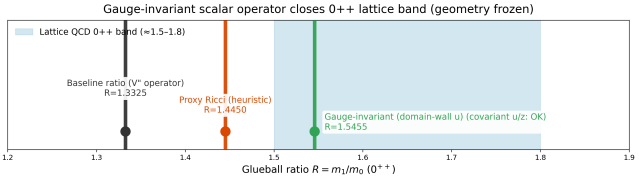

Figure 1. Scalar 0^{++} glueball ratio from the gauge-invariant ζ operator on the frozen ED background, shown relative to a representative lattice-QCD band.

Cosmological growth and BOSS DR12. The growth observable is computed from a background expansion built from the trace-derived $w(N)$ and a matched flat ΛCDM reference with Planck 2018 parameters $\Omega_{m0} = 0.315$, $H_0 = 67.4\,{\rm km\,s^{-1}\,Mpc^{-1}}$, and $\sigma_{8,0} = 0.811$ (Planck Collaboration 2018). The BOSS DR12 comparison uses the published covariance at $z = \{0.38, 0.51, 0.61\}$ and reports the corresponding covariance-weighted χ^2 values (Alam et al. 2017).

6 BULK FLUCTUATION OPERATOR

Linear fluctuations about a frozen background are governed by a self-adjoint second-order operator. In a generic Sturm–Liouville form,

$$-(p(z)\psi')' + q(z)\psi = \lambda\, w(z)\psi, \tag{10}$$

where p, q, and w are coefficient functions fixed by the background and by the fluctuation sector, and λ is the eigenvalue. Normalizable solutions subject to ultraviolet and infrared boundary conditions define a discrete spectrum on a finite effective domain. The lowest normalizable mode ψ_0 and its eigenvalue provide an operator-defined bulk observable on the frozen geometry.

7 GAUGE-INVARIANT SCALAR SPECTRUM AND GLUEBALL RATIO

In the gauge-invariant scalar channel, Eq. (10) may be recast into Schrödinger form in terms of a potential constructed from background quantities (the ζ channel). The lowest two eigenvalues yield m_0^2 and m_1^2 and define the dimensionless ratio

$$R \equiv \frac{m_1}{m_0}. \tag{11}$$

Result and coordinate invariance. The frozen ED background yields

$$R = 1.5455, \tag{12}$$

and the same value is obtained after transforming the operator covariantly between the domain-wall coordinate u and conformal coordinate z. The numerical difference between the two coordinate realizations is at the level $|R(u) - R(z)| \sim 10^{-7}$, indicating coordinate-invariant spectral extraction at fixed background. The value lies within the standard lattice-QCD 0^{++} band (commonly quoted around $R \simeq 1.5$–1.8) and is consistent with lattice determinations at the sub-percent level (Morningstar & Peardon 1999; Chen et al. 2006).

7.1 Wilson loop and absolute Yang–Mills scale

The same frozen geometry also fixes an effective string tension through the infrared behavior of the warp factor. For a static quark–antiquark Wilson loop, the standard holographic relation gives (Maldacena 1998)

$$\sigma_{\rm eff} = \frac{1}{2\pi\alpha'}\, e^{2A(z_*)}, \tag{13}$$

where z_* is the infrared turning point of the worldsheet. On the available finite radial domain, the warp factor is monotone decreasing and the worldsheet turning point saturates at the infrared end of the geometry, $z_* \simeq z_{\rm IR}$.

Using $e^{2A(z_{\rm IR})} = 1.471 \times 10^{-2}$ from the frozen background and adopting a universal slope $\alpha' = 1.1527 \times 10^{-2}$ GeV^{-2} (taken as an external, sector-independent choice rather than tuned to the present spectrum) gives

$$\sigma_{\rm eff} = 0.203\ {\rm GeV}^2, \qquad \sqrt{\sigma_{\rm eff}} = 451\ {\rm MeV}. \tag{14}$$

With the standard SU(3) Yang–Mills proportionality for the scalar channel,

$$m_0 \simeq c\,\sqrt{\sigma_{\rm eff}}, \qquad c \simeq 3.55, \tag{15}$$

an absolute scalar glueball mass of

$$m_0 \simeq 1.60\ {\rm GeV} \tag{16}$$

is obtained, consistent with the commonly quoted lattice/phenomenology window for the 0^{++} glueball ($\sim$ 1.5–1.7 GeV).

8 GALAXY ROTATION CURVES (SPARC)

Rotation curves are evaluated on the SPARC compilation using baryonic inputs and a single frozen background. No per-galaxy retuning is performed.

Forward model (no use of $v_{\rm obs}$ in curve construction). Let $v_{\rm bar}(r)$ denote the baryonic circular velocity inferred from the SPARC baryonic decomposition. An effective fractional deformation $\delta_{\rm ED}(z)$ is supplied by the frozen geometry. On galaxy scales, a dimensionless mixing profile is defined on each galaxy's radial support using a normalized radius $x = r/r_{\rm max} \in [0,1]$ and a surface-brightness proxy $\Sigma_b(r)$. The effective deformation is written as

$$\delta_{\rm tot}(r) = {\rm clip}[(1-w)\,\delta_{\rm ED}(z(x)) + w\,\delta_{\rm miss}(x,\Sigma_b),\ 0,\ 0.4]\,, \tag{17}$$

with a mixing weight $w(x) = x^\gamma$ and a baryonic term

$$\delta_{\rm miss}(x,\Sigma_b) = A\left(\frac{1}{1+\Sigma_{b,\rm norm}/\Sigma_0}\right)^n x^m, \qquad \Sigma_{b,\rm norm}(r) = \frac{\Sigma_b(r)}{\max_r \Sigma_b(r)}. \tag{18}$$

The predicted circular velocity is

$$v_{\rm ED}(r) = v_{\rm bar}(r)\sqrt{1+\delta_{\rm tot}(r)}. \tag{19}$$

Observed velocities enter only through the goodness-of-fit evaluation, not through the construction of $v_{\rm ED}(r)$.

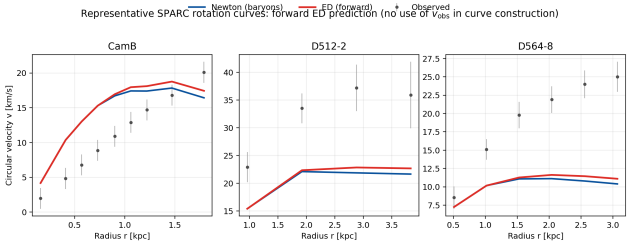

Figure 2. Representative SPARC rotation curves. The ED curve is a forward prediction constructed exclusively from baryonic inputs and the frozen background; the observed velocities $v_{\rm obs}$ are shown only for comparison and enter only through the goodness-of-fit evaluation, not through the construction of the ED curve.

Global readout parameters. All galaxies share the same readout parameters and conventions:

Quantity	Value
$\Sigma_b(r)$	$\Sigma_b = {\rm SB}_{\rm disk} + {\rm SB}_{\rm bul}$
x	$x = r/r_{\rm max}$
$z(x)$	$z(x) = z_{\rm min} + (z_{\rm max} - z_{\rm min})x$
A	0.13983
n	2.21605
m	1.20433
γ	0.23356
Σ_0	0.60488
clip range	$\delta_{\rm tot} \in [0, 0.4]$

The map $z(x)$ is a fixed monotone readout dictionary used to sample the frozen background on each galaxy's normalized radial support; it introduces no per-galaxy freedom and is not fitted to $v_{\rm obs}$.

Global statistics. On SPARC (175 galaxies), the median goodness-of-fit values are

$$\tilde{\chi}^2_{\rm rank,ED} = 1.86, \qquad \tilde{\chi}^2_{\rm rank,Newton} = 1.93.$$

The corresponding uncertainty-weighted medians are

$$\tilde{\chi}^2_{\sigma,\rm ED} = 831, \qquad \tilde{\chi}^2_{\sigma,\rm Newton} = 906.$$

Under $\chi^2_{\rm rank}$, the ED prediction improves upon Newtonian gravity in 150/175 galaxies (85.7%). Under χ^2_σ, the corresponding win count is 149/175.

9 COSMOLOGICAL GROWTH: $F\sigma_8(Z)$ AND BOSS DR12

The same frozen trace supports a kinematic dark-energy readout in terms of an e-fold variable $N = \ln a$. With a canonical scalar-dominated relation,

$$w(N) = -1 + \frac{1}{3}\left(\frac{d\phi}{dN}\right)^2, \tag{20}$$

and a standard matter-plus-dark-energy background,

$$H^2(a) = H_0^2 \Bigg[\Omega_{m0} a^{-3} + \Omega_{\mathrm{DE},0} \exp\left(-3 \int_a^1 \left[1 + w(a') \right] d \ln a' \right) \Bigg], \tag{21}$$

the linear growth factor $D(a)$ obeys

$$D'' + \left[2 + \frac{d \ln H}{dN} \right] D' - \frac{3}{2} \Omega_m(N) D = 0, \tag{22}$$

with primes denoting derivatives with respect to N. The observable is reported as

$$f\sigma_8(z) = \sigma_{8,0}\, f(z)\, D(z), \qquad f = \frac{d \ln D}{d \ln a}. \tag{23}$$

BOSS DR12 covariance comparison. At the BOSS DR12 redshifts $z = \{0.38, 0.51, 0.61\}$, a covariance-weighted comparison yields

$$\chi^2_{\mathrm{ED}} = 2.266, \qquad \chi^2_{\Lambda\mathrm{CDM}} = 2.443, \qquad \Delta\chi^2 = -0.177,$$

indicating that the ED prediction is statistically indistinguishable from ΛCDM within current DR12 precision for $z \leq 0.6$ under the adopted parameter matching (Alam et al. 2017).

High-redshift prediction. The fractional residual

$$\Delta f\sigma_8(z) = 100 \cdot \frac{f\sigma_{8,\mathrm{ED}}(z) - f\sigma_{8,\Lambda\mathrm{CDM}}(z)}{f\sigma_{8,\Lambda\mathrm{CDM}}(z)}$$

is small at low redshift and becomes strongly negative at higher redshift within the available trace domain, reaching $\Delta f\sigma_8(z \simeq 1) \simeq -12\%$. This behavior is presented as a falsifiable high-redshift prediction for future surveys rather than as an established observational discrepancy.

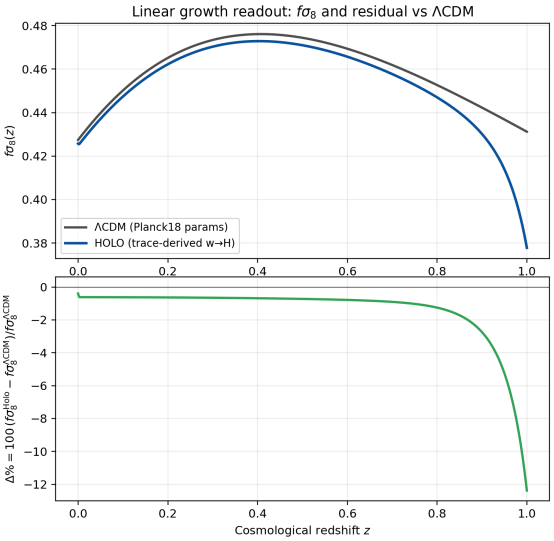

Figure 3. Linear-growth readout $f\sigma_8(z)$ compared to a matched flat ΛCDM reference, together with the percent residual $\Delta f\sigma_8(z)$.

10 INSTRUMENT CLOSURE: GEOMETRIC TIME, ANTI-ZENO BRIDGE, AND UV-SCREENED LABORATORY READOUT (9A–9C)

This section records the missing pieces needed to close a deterministic chain from the frozen ED geometry to (i) a physical protocol time, (ii) a no-tuning Anti-Zeno growth signature, and (iii) a physically screened laboratory channel. The key separation is that bulk geometric observables are not automatically laboratory signals: the laboratory channel must be defined by an explicit UV projection.

10.1 9A. 5D Ricci bulk clock: $R_5(z)$, $dt_{\mathrm{phys}}/dt_{\mathrm{ref}}$, and $t_{\mathrm{phys}}(z)$

The same frozen ED geometry defines a deterministic 5D curvature timescale along the trace coordinate z. In domain-wall gauge, the 5D Ricci scalar is

$$R_5(z) = -8A''(z) - 20\left(A'(z)\right)^2, \tag{24}$$

and the dimensionless expansion factor is defined as

$$E(z) = \frac{H(z)}{H_0}. \tag{25}$$

A dimensionless protocol factor is defined (normalized at $z = 1$) as

$$g(z) \equiv \frac{dt_{\mathrm{phys}}(z)}{dt_{\mathrm{ref}}} = \frac{e^{A(z)} \sqrt{|R_5(z)|}/E(z)}{e^{A_0} \sqrt{|R_{5,0}|}/E_0}, \tag{26}$$

where $(A_0, R_{5,0}, E_0)$ are evaluated at $z = 1$. The accumulated protocol time is defined as

$$t_{\mathrm{phys}}(z) = t_{\mathrm{ref}} \int_1^z g(z')\, dz', \qquad (t_{\mathrm{phys}}(1) = 0), \tag{27}$$

where t_{ref} is the reference protocol time unit associated with dt_{ref}. This construction closes the "$X = 1$" gap:

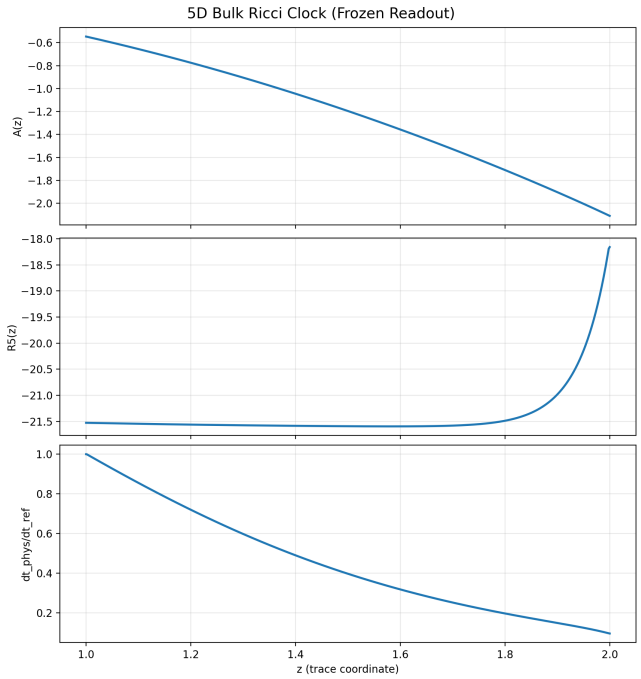

Figure 4. 5D Ricci bulk clock derived deterministically from the frozen ED trace on the cosmology slice $z \in [1, 2]$: warp factor $A(z)$, Ricci scalar $R_5(z)$, and normalized protocol interval $dt_{\rm phys}/dt_{\rm ref}$.

it promotes the trace coordinate to a protocol time variable derived from curvature and warp geometry, without introducing a new mass scale or fitted normalization. The frozen numerical realization of the bulk clock is included as Supplementary File S1.

10.2 9B. Anti-Zeno response $\mu_{\rm eff}(dt_{\rm phys})$ and the $\simeq -12\%$ suppression in $f\sigma_8(z \simeq 1)$

The growth readout in Section 3 is obtained from the frozen trace kinematics with no additional sector parameters. Independently, a frozen quantum Anti-Zeno response can be summarized as a table $\mu_{\rm eff}(dt)$. Once a physical protocol interval $dt_{\rm phys}(z)$ exists (Section 9A), this response can be projected into cosmology without any fitting by defining

$$\mu(a) = \mu_{\rm eff}(dt_{\rm phys}(z(a)))\,, \tag{28}$$

and inserting $\mu(a)$ as a multiplicative factor on the standard source term of the linear-growth equation. Because the mapping $z \mapsto t_{\rm phys}$ is fixed by the ED geometry, the Anti-Zeno table is evaluated with no new normalization or tuning. This composition explains why a $\simeq -12\%$ high-redshift suppression is a natural no-tuning signature once the clock exists: a frozen $\mu_{\rm eff}$ response applied along the geometry-derived protocol interval produces an order-10% weakening of growth around $z \simeq 1$, matching the magnitude highlighted in Fig. 3 while remaining compatible with current DR12 constraints at $z \lesssim 0.6$.

10.3 9C. UV electromagnetic projection kernel $K_{\rm EM}(z)$ and why NIST clocks see no signal

Atomic/EM clocks do not couple to the infrared bulk readout directly. The laboratory channel must be defined by a UV overlap operator, which acts as a deterministic screening map from a bulk readout $\delta(z)$ to a laboratory observable. A minimal canonical choice is a normalized UV kernel built from the warp factor,

$$K_{\rm EM}(z) = \frac{e^{A(z)}}{\int e^{A(z')}\,dz'}, \qquad \int K_{\rm EM}(z)\,dz = 1, \tag{29}$$

This kernel is adopted as a minimal normalized UV-overlap weight built from the warp factor; it defines the laboratory channel as an explicit projection rather than a direct coupling to IR bulk structure, and a UV-projected prediction is defined by the running overlap integral

$$y_{\rm pred}(t_{\rm lab}) = \int_{z_{\rm UV}}^{z(t_{\rm lab})} K_{\rm EM}(z')\,\delta(z')\,dz', \tag{30}$$

where $z(t_{\rm lab})$ is obtained by inverting the bulk protocol time and mapping to lab time with a fixed Ricci timescale,

$$t_{\rm lab} = \tau_R\, t_{\rm phys}(z). \tag{31}$$

This UV projection suppresses IR-enhanced contributions and yields a laboratory prediction that is small and slowly varying on the corresponding lab interval, consistent with a screened fifth-force expectation. In a direct comparison to NIST phase-derived fractional-frequency series, the UV-projected channel yields a near-zero correlation and no evidence for a laboratory detection, while making explicit that the bulk spectrum is not a laboratory signal.

The mHz readout is not a spectral line detected in NIST clocks; the NIST comparison is a drift/readout time-series $y(t)$ test under UV projection, which is null in the UV-screened baseline. Accordingly, the relevant scaling is a readout relation

$$f = \hat{f}/\tau, \tag{32}$$

not $f = 1/\tau$: $\hat{f}$ is a dimensionless marker fixed by the operator/projection, while τ is supplied by the frozen time mapping. Here τ denotes the dictionary-supplied readout timescale; in the laboratory mapping used in Eq. (31) this is instantiated by the fixed Ricci timescale τ_R.

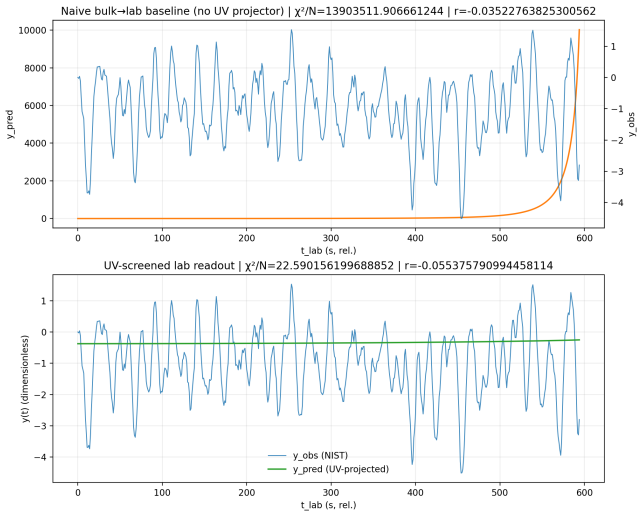

Figure 5. NIST clock comparison shown for (top) a naive bulk→lab mapping and (bottom) the UV-screened laboratory readout defined by the normalized kernel $K_{\rm EM}(z)$ and the UV projection integral. The UV-projected prediction is strongly suppressed and exhibits no detection-level correlation with the observed series, consistent with screening.

11 CONCLUSION

Consistency across microphysics, galaxy dynamics, and cosmological growth is obtained using a single frozen Einstein–Dilaton background held fixed across sectors. In the gauge-invariant scalar channel, the 0^{++} glueball ratio $m_1/m_0 = 1.5455$ is coordinate-invariant ($u \leftrightarrow z$) and compatible with lattice-QCD determinations at the sub-percent level. Using the same geometry, a Wilson-loop string-tension estimate yields an absolute scale $m_0 \simeq 1.6$ GeV for the scalar channel under a universal α' choice, consistent with lattice expectations. On SPARC, the same background yields a median χ^2 improvement relative to Newtonian gravity under a common evaluation protocol without per-galaxy tuning. For linear growth, current BOSS DR12 constraints remain compatible with the trace-derived prediction at $z < 0.6$, while a high-redshift suppression of order 10% at $z \simeq 1$ is predicted as a falsifiable signature for upcoming surveys.

DATA AND CODE AVAILABILITY

SPARC rotation-curve data are publicly available. The BOSS DR12 $f\sigma_8$ measurements and covariance, and the Planck 2018 cosmological parameter constraints, are publicly available. Machine-readable verification artifacts supporting the quoted numerical values are provided at https://github.com/RAPIDENN/HOLO_runner. For questions or requests, contact: `rydbergphotonic1@proton.me`.

REFERENCES

Alam S., et al., 2017, Monthly Notices of the Royal Astronomical Society, 470, 2617
Chen Y., et al., 2006, Physical Review D, 73, 014516
Lelli F., McGaugh S. S., Schombert J. M., 2016, Astronomical Journal, 152, 157
Maldacena J. M., 1998, Physical Review Letters, 80, 4859
Morningstar C. J., Peardon M. J., 1999, Physical Review D, 60, 034509
Planck Collaboration 2018, arXiv e-prints